Published in final edited form as:
Heart Rhythm. 2012 November ; 9(11): 1855–1862. doi:10.1016/j.hrthm.2012.07.003.

Intracardiac Acoustic Radiation Force Impulse Imaging: A Novel Imaging Method for Intraprocedural Evaluation of Radiofrequency Ablation Lesions:

Feasibility of intraprocedure ARFI imaging of RFA

Stephanie A. Eyerly, M.S.,
Department of Biomedical Engineering, Duke University, Durham, NC, USA

Tristram D. Bahnson, M.D.,
Duke Center for Atrial Fibrillation, Duke Heart Center, and Clinical Cardiac Electrophysiology Section of the Division of Cardiovascular Medicine, Duke University, Durham, NC, USA

Jason I. Koontz, M.D., Ph.D.,
Duke Center for Atrial Fibrillation, Duke Heart Center, and Clinical Cardiac Electrophysiology Section of the Division of Cardiovascular Medicine, Duke University, Durham, NC, USA

David P. Bradway, B.S.,
Department of Biomedical Engineering, Duke University, Durham, NC, USA

Douglas M. Dumont, Ph.D.,
Department of Biomedical Engineering, Duke University, Durham, NC, USA

Gregg E. Trahey, Ph.D., and
Department of Biomedical Engineering, Duke University, Durham, NC, USA; Department of Radiology, Duke University Medical Center, Durham, NC, USA

Patrick D. Wolf, Ph.D.
Department of Biomedical Engineering, Duke University, Durham, NC, USA

Abstract

Background—Arrhythmia recurrence after cardiac radiofrequency ablation (RFA) for atrial fibrillation (AF) has been linked to conduction through discontinuous lesion lines. Intraprocedural visualization and corrective ablation of lesion line discontinuities could decrease post-procedure AF recurrence. Intracardiac acoustic radiation force impulse (ARFI) imaging is a new imaging technique that visualizes RFA lesions by mapping the relative elasticity contrast between compliant-unablated and stiff-RFA treated myocardium.

Objective—To determine if intraprocedure ARFI images can identify RFA treated myocardium *in vivo*.

Editorial Correspondence and Reprint Requests to: Patrick Wolf, Department of Biomedical Engineering, Duke University, 136 Hudson Hall, P.O. Box 90281, Durham, NC 27708, Phone: 919.660.5114, Fax: 919.684.4488, patrick.wolf@duke.edu.

Potential Conflicts of Interest: This study used loaned equipment from Siemens© Healthcare (ACUSON S2000™ ultrasound scanner: Issaquah, WA) and Biosense Webster®, Inc. (CARTO® XP EP Navigation System: Diamond Bar, CA). Gregg Trahey reports relevant patent application and ownership.

Methods—In eight canines, an electroanatomical mapping (EAM) guided intracardiac echo catheter (ICE) was used to acquire 2D ARFI images along right atrial ablation lines before and after RFA. ARFI images were acquired during diastole with the myocardium positioned at the ARFI focus (1.5 cm) and parallel to the ICE transducer for maximal and uniform energy delivery to the tissue. Three reviewers categorized each ARFI image as depicting no lesion, non-contiguous, or contiguous lesion. For comparison, three separate reviewers confirmed RFA lesion presence and contiguity based on functional conduction block at the imaging plane location on EAM activation maps.

Results—Ten percent of ARFI images were discarded due to motion artifacts. Reviewers of the ARFI images detected RFA-treated sites with high sensitivity (95.7%) and specificity (91.5%). Reviewer identification of contiguous lesion had 75.3% specificity and 47.1% sensitivity.

Conclusions—Intracardiac ARFI imaging was successful in identifying endocardial RFA treatment when specific imaging conditions were maintained. Further advances in ARFI imaging technology would facilitate a wider range of imaging opportunities for clinical lesion evaluation.

Keywords

ARFI imaging; transcatheter cardiac radiofrequency ablation; lesion assessment; atrial fibrillation

Introduction

Radiofrequency ablation (RFA) is an established curative therapy for cardiac arrhythmias.[1] Transcatheter ablation (TCA) for atrial fibrillation (AF) electrically isolates arrhythmogenic regions of the atria by creating contiguous and transmural lines of multiple discrete lesions with radiofrequency energy. Therefore, lesion placement and line contiguity are important determinants of procedure efficacy.[1–3]

To date, there is no clinically proven method to visually evaluate the presence or extent of RFA lesions during TCA. Electroanatomical mapping (EAM) systems guide lesion placement, annotate the catheter position during RF energy delivery, and construct substrate conduction maps. EAM conduction maps provide indirect feedback about lesion formation during RFA, but cannot provide direct lesion visualization. Fluoroscopy and intracardiac ultrasound imaging (ICE) can guide catheter placement during TCA, but lack the soft tissue contrast needed to provide lesion assessment.[4] Intraprocedural visualization of RFA lesions could improve TCA outcomes by identifying incomplete RFA lesion formation and guiding additional ablation to complete the lesion set.

Acoustic radiation force impulse (ARFI) imaging is a novel ultrasound-based technique that creates 2D images of relative tissue elasticity.[5] ARFI imaging uses ultrasonic radiation force impulses to mechanically displace tissue and conventional ultrasound methods to monitor the tissue response spatially and temporally. The displacement magnitude (~10μm) is calculated using correlation-based delay estimation methods.[6,7] The magnitude of the tissue displacement is inversely proportional to tissue elasticity, and a 2D image of ARFI-induced tissue displacement provides visualization of relative tissue stiffnesses.[8, 9]

RF-induced tissue heating causes irreversible thermocoagulation and permanently denatures intracellular and contractile proteins which increases tissue stiffness.[10–12] We have previously demonstrated that ICE-based ARFI imaging can visualize the relative elasticity difference between ablated and unablated myocardium *in vivo* and can accurately assess focal RFA lesion morphology *in vitro*.[13–15]

As currently implemented, 2D ICE-based ARFI images can be acquired and displayed every few seconds; this frame rate makes it difficult to "scan" the heart for lesions. ICE-based ARFI imaging can be integrated with EAM to guide the ARFI imaging plane to RFA annotated areas enabling efficient intraprocedure lesion evaluation.

This animal study was undertaken to determine if intracardiac ARFI imaging can be used to detect RFA treatment and evaluate conduction block producing contiguous lesion lines during *in vivo* TCA.

Methods

Integrated Imaging System and Procedural Equipment Setup

The multi-modality imaging system consisted of a modified CARTO XP EP Navigation System (Biosense Webster; Diamond Bar, CA) and a software modified Siemens ACUSON S2000 ultrasound scanner (Siemens Healthcare; Issaquah, WA). A custom CARTOSound module (Biosense Webster; Software Development, Tirat Carmel, Israel) was installed to display the S2000 ICE image in the CARTO XP software. Conventional ICE and ARFI images were acquired with a commercially available 10 French SoundStar catheter without modification (Biosense Webster). ARFI images were acquired and displayed on a laptop computer (Dell Precision M90) within 15 seconds during the procedure.

Catheters were navigated to the heart with fluoroscopy (C-Arm, Philips Healthcare; Andover, MA). All focal RFA lesions were delivered with a Stockert 70 Generator and NaviStar mapping/ablation catheter (Biosense Webster) with a peak energy of 30 to 45 Watts under temperature control with a target temperature between 50–60° C for ~30–90 seconds. An octapolar sensing catheter (XT Steerable, Bard; Lowell, MA) was positioned in the coronary sinus (CS) and the distal electrodes were used as the activation mapping reference and pacing electrodes (S48 Square Pulse Stimulator, Grass Technologies; West Warwick, RI).

The surface ECG and endocardial electrograms (EGs) from the sensing and mapping catheters were acquired by the CARTO patient interface unit (PIU), input into an Octal Bio Amp (ADInstruments; Milford, MA), and recorded using LabChart 7.0 data acquisition software (PowerLab, ADInstruments). In LabChart, an output channel was configured to provide an impulse at a user selected delay after a detected QRS of the ECG. This signal was fed into the ultrasound scanner as a pseudo-ECG and used to gate the image acquisitions.

Animal Experiment Procedure

The animal study protocol was approved by the Duke University Animal Care and Use Committee and conformed to the Guide for the Care and Use of Laboratory animals.[16]

Eight canine subjects were anesthetized (pre-anesthesia: intramuscular acepromazine 0.02–0.05 mg/kg followed by interveinous propofol 4–6 mg/kg; general anesthesia: isoflurane gas 1–5% via inhalation), intubated, ventilated and maintained metabolically stable. A baseline point-by-point geometry and LAT-map was made of the canine right atrium (RA). A pre-RFA guideline of points delineating the intended sites of ablation was drawn on the CARTO LAT map; baseline ARFI images were acquired along this guideline. The ICE fan position and orientation for each ARFI imaging location was saved for post-procedure review using the navigation features of the EAM system. Discrete RFA lesions were delivered along the guideline in two stages. The first stage left an intentional ~1 cm gap, and the gap was closed in the second stage. After each stage, a new LAT-map was constructed and the ablation line was ARFI imaged. At the end of the study, the animal was euthanized and the heart was

removed to confirm lesion delivery. The RFA lesions were photographed with a digital camera.

In vivo ARFI Imaging Implementation

The ARFI images were created using a standard 64-element SoundStar catheter imaging at 6.15MHz (1.5cm focus). The S2000 ultrasound scanner was software-modified to implement 2D beam sequences that acquire spatially and temporally registered B-mode and ARFI images. A single ARFI image covered a 37° FOV and required ~92 ms to acquire. Image data acquisition, data transfer, data processing, and image display took approximately 10–15 seconds per ARFI image. All imaging sequences used were within regulatory limits for mechanical index (MI <1.7) and transducer surface heating (<4.0° C).[17]

In this study, ARFI images were acquired with the myocardium positioned near the ARFI imaging focus (1.5 cm) and parallel to the ICE transducer. ARFI imaging of the myocardium outside the appropriate imaging depth of field (DOF, between 0.5 cm and 2.25 cm) substantially reduces the acoustic energy delivered to the tissue and subsequently the relative elasticity contrast.[14] ARFI imaging the endocardial surface at an oblique angle creates non-uniform acoustic energy delivery into the tissue, resulting in depth dependent differences in relative tissue elasticity. Any ARFI images where the myocardial surface was outside the DOF or at an oblique angle (>50°) were discarded. Lastly, ARFI images with the mapping catheter in the field of view (FOV) were excluded from analysis because the catheter tip blocked acoustic energy from entering the tissue, creating a shadowing artifact.

All ARFI acquisitions in this experiment were also ECG-gated and acquired during diastole using the adjustable LabChart output channel. ARFI imaging during diastole reduces artifacts caused by cardiac motion; bulk motion of the myocardium during the acquisition can corrupt the tissue displacement measurements.[13,14] Acquisitions were also gated to diastole to maximize the stiffness contrast between RFA lesions and the surrounding unablated myocardium.[13,14,18] To demonstrate the elasticity contrast between systole and diastole in ARFI imaging, figure 1A presents ARFI images (acquired with a VF10-5 linear transducer, Siemens Healthcare) of a ventricular epicardial RFA lesion at different times in the cardiac cycle. The lesion is visible as a semicircular region of relatively low ARFI-induced displacement. The ARFI image stiffness contrast between the lesion and unablated myocardium is maximal during diastole (figures 1A-1 and 1A-4). The larger 128-element ultrasound transducer was used for this demonstration because it allowed a fast imaging frame rate (14 Hz) to observe the stiffening of the myocardium. Frame rates this high damage existing intracardiac probes.

ARFI Image Processing

The 2D ARFI images were formed by delivering acoustic impulses to the tissue and tracking the resulting displacement for ~1 ms at each pixel using the normalized cross-correlation methods outlined by Hsu *et al.*[14] Regions of the image with poor displacement estimates (blood, tissue beyond the DOF) were removed by thresholding the median normalized cross-correlation coefficient. Pixel locations with a large displacement standard deviation (>1μm) through the tracking period were also removed. A quadratic extrapolation motion filter was applied to the raw ARFI image data to reduce the effects of bulk physiological motion and catheter rebound on the displacement estimates.[7, 14] The maximum ARFI-induced displacement for each pixel location throughout the tracking time were combined to create a single 2D maximum ARFI-induced displacement image. Upon completion of the image processing, ARFI images that exhibited substantial motion artifacts such as low normalized cross-correlation coefficients within the myocardium (<0.75) or visible myocardial discontinuity were not included in the final statistical analysis.

For the final display, the upper limit of the ARFI displacement color bar was initially set to 10μm and manually adjusted to increase contrast and reduce saturation. The lower limit of the color bar was always set to 0μm. Energy delivery was maximal at the focus, and the color bar range was typically increased for images where the myocardium was directly at the focus and decreased when it was located above or below the focus. The range for all images of the upper-limit of the color bar was 7.5– 15μm.

EAM LAT Maps

Screenshots of each imaging fan position were compiled with the LAT-map using the CARTOSound Module in the system Review Mode. The tricuspid annulus (TA) was cut from the map, and internal points were removed. The ablation and guideline markers were hidden, and the color scale of each LAT-map was adjusted to increase the color gradient at the ablation line.

Image Review and Statistical Analysis

The ARFI images and their corresponding LAT-maps were separately randomized and each read by three different reviewers (six total reviewers).

Three reviewers (all experienced in ARFI imaging) were instructed to classify the ARFI images into one of three categories: 1) *no lesion,* defined as the ARFI image depicts no visible area of low relative displacement in the myocardium, 2) *non-contiguous lesion*, depicts at least one area of low relative displacement that does not extend the entire length or depth of the imaged myocardium, or 3) *contiguous lesion*, the full extent of the imaged myocardium depicts low relative displacement.

Three different reviewers (two clinical electrophysiologists, one electrophysiology expert) were posed three yes or no questions about each LAT-map in reference to the baseline map: 1) "*Is there conduction block anywhere on this LAT-map?"* (additional possible answer of "Cannot be determined"), 2) "*Based on the activation pattern in the LAT map, does there appear to be RF lesions present at the ICE imaging fan location?"*, and 3) "*Is the ICE imaging plane completely parallel to and transecting a line of block, thereby imaging a continuous line of lesion?"*. The RFA lesion widths observed in the postmortem pathology photographs were typically between 4 and 8mm; therefore, questions #2 and #3 were answered considering the imaging plane could be transecting RFA lesions within ~8mm of conduction block.

The degree of the agreement within the sets of three reviewers was quantified with the kappa statistic.[19] The majority (at least 2 of 3 reviewers) reviews for both the ARFI images and LAT-maps were used to determine the final image-map pair assessment. Image pairs where the LAT-map assessment had no majority review or the majority review misidentified the correct stage of ablation (question #1, pre vs. post RFA) were also removed from the analysis.

Heterogeneity analysis was performed to justify pooling the data for all animals. A heterogeneity chi-square statistic was calculated to confirm that the data from the different animals came from a homogeneous population.[20]

The majority ARFI image categorization and LAT-map assessment from question #2 were used to compile a 2×2 contingency table of all image pairs to summarize the ability of ARFI imaging to identify RFA lesion. For the ARFI images, the category "Lesion" included the non-contiguous and continuous classifications. A second 2×2 contingency table was compiled to summarize the ability of ARFI imaging to identify lesion line discontinuities and conduction block using the LAT-map assessments from questions #2 and #3. This table

only included post-ablation image pairs with a yes response to LAT-map assessment question #2. The sensitivity, specificity, positive predictive value (PPV), and negative predictive value (NPV) were calculated for both tables.

Results

In eight canine subjects, 243 ARFI images were acquired with the outlined imaging conditions. Twenty-four images were rejected due to motion artifact; the remaining 219 ARFI image-LAT map pairs (54 pre-ablation, 80 after incomplete ablation, and 85 after gap closure) were reviewed for statistical analysis. The kappa coefficient for the ARFI image assessments indicated substantial agreement ($\kappa = 0.734$) between the three reviewers. The individual kappa coefficients for the LAT-map review questions showed almost perfect agreement when reading for global conduction block ($\kappa = 0.909$), substantial agreement for identifying lesions at the imaging plane ($\kappa = 0.684$), and moderate agreement when assessing full conduction block at the imaging plane ($\kappa = 0.428$). The LAT-map reviewers had different question responses (no majority review) for 15 image pairs. The majority review misidentified the correct stage of ablation in five LAT-maps. These 20 image pairs we excluded from the final analysis.

The statistical calculations included 199 image pairs. The reviews for detecting RFA treatment with ARFI imaging compared to the reviews for identifying conduction disturbance in the LAT-map is shown in Table I. Table II shows the ARFI image reviews for RFA lesion contiguity vs. functional conduction block (n=140, includes only post ablation image pairs confirmed by the LAT-map review). The heterogeneity analysis justified pooling the data from all the animal subjects. Table III summarizes the heterogeneity chi-square and p-value, sensitivity, specificity, PPV, and NPV for Tables I and II.

An image pair example from each ablation stage is shown in figure 2. Before RFA (figure 2C-1) the myocardial elasticity is homogeneous with relatively high ARFI-induced displacements. Figure 2C-2 shows the unablated gap in the lesion line, visible as the area of high tissue displacement (>7.5μm) surrounded by areas of relatively low tissue displacements (<4.5μm). The final ARFI image (figure 2C-3) shows a homogeneous region of low displacement, confirming complete ablation of the gap.

Discussion

This study demonstrated that ARFI imaging, a new ultrasound-based elasticity imaging technique, has the potential to provide intraprocedure visualization of endocardial RFA lesions during TCA. RFA lesions were identified as regions with low ARFI-induced tissue displacement, indicating increased stiffness, in contrast to the relatively high displacement of unablated myocardium. Conduction disturbances at the imaging site on the LAT-maps confirmed RFA treatment. Reviewers of the ARFI images accurately detected RFA treated areas from non-treated areas with high sensitivity, specificity, and predictive values. Reviewers also distinguished unablated gaps between adjacent RFA lesions that corresponded to conduction “breakthrough” on the activation map. Furthermore, ARFI images reviewed as contiguous RFA frequently displayed conduction block on the activation map. Overall, we believe using intracardiac ARFI imaging for intraprocedural elasticity-based lesion evaluation is feasible and merits further investigation.

Clinical Translation and Implications

Lesion evaluation with an ARFI imaging-EAM system could guide the delivery of consolidating RFA to lesion line discontinuities and subsequently decrease the total procedure time and increase the success rate of procedures that use linear ablation strategies,

such as pulmonary vein isolation (PVI). An ARFI imaging-EAM system uses existing clinical tools and techniques, therefore clinics would not need to purchase and install expensive new equipment in the operating rooms and electrophysiologists would not need significant training to use the system.

As implemented in this study, the primary difficulty for translating intracardiac ARFI imaging to clinical practice is the specific imaging conditions required to create usable ARFI images. The ICE catheter must be within 2 cm of the myocardium or the tissue cannot be detectably displaced by the acoustic impulse, and the endocardial surface must be nearly parallel to the transducer or the uneven distribution of radiation force leads to spatial differences in displacement unrelated to the relative tissue elasticity. Future work to prepare ARFI imaging for widespread clinical adoption could include the production of an ICE catheter with a transducer optimized for ARFI imaging to increase the imaging DOF and developments in ARFI imaging sequencing and image processing methods for energy-depth normalization when imaging curvilinear surfaces. Also, current intracardiac ARFI imaging technology limits the imaging rate to 3 or 4 acquisitions per minute. Improvements for near real-time imaging will have to balance increasing acquisition rates against increasing acoustic exposure (MI/transducer face heating).

Finally, imaging was gated to diastole to minimize motion artifacts and the ARFI-induced displacement data was motion filtered to reduce the effects of axial bulk motion on the displacement estimations. Unfortunately, as seen in ~10% of acquired images in this study, motion artifacts can occur if the acquisition is mistimed due to changes in heart rate or if the tissue motion is perpendicular to the imaging plane. Experience and the development of more sophisticated gating techniques could reduce the incidence of motion artifacts in the images. Also, the canine heart rates (often >120 beats per minute) were higher than typical human patients; slower heart rates provide a longer diastolic window for imaging, subsequently reducing the frequency of mistimed acquisitions. However, it is unknown how the inability to ECG-gate imaging during AF will affect ARFI image quality and contrast. Despite the limitations, a substantial number of high quality images of ablation lesions were obtained *in vivo* and some clinicians may find utility in the technique even without significant advances in the imaging technology.

Distinguishing Conductive from Non-Conductive Unablated Gaps

Cardio-myocytes near sites of RFA delivery can be reversibly “stunned” so that conduction block is observed acutely after circumferential or antral PV isolation only to recover at some later time; the reconnection of the PVs is believed to be an important factor limiting the efficacy of TCA for AF.[21–23] The discordance between the activation defined completeness of conduction block and the ARFI imaging defined lesion contiguity described here could potentially be explained by the indirect functional vs. direct imaging method of assessing block. Further investigation will be required to show that imaging tissue stiffness is a more sensitive measure of ablation lesion durability and long-term ablation success than acute activation mapping.

In addition to electrical stunning, edema occurs within RFA treated regions.[24] Edema can stiffen the myocardium, and it is unclear whether ARFI imaging is able to differentiate stiffening due to edema from RF-induced coagulation necrosis of the cardiac tissue. This study indicated ARFI imaging could detected lesion line discontinuities, but further study of the change in stiffness due to substantial fluid swelling in conductive gaps between RFA lesions is needed.

Study limitations

The gold-standard for image validation is the examination of the tissue pathology. Unfortunately, manually matching the exact orientation and location of each 2D ARFI imaging plane to the *ex vivo* pathology would risk substantial misregistration error that would affect the accuracy of the lesion evaluations. EAM is the current end-procedure gold-standard for assessing ablation line completeness, therefore this study used EAM to identify regions of conduction disturbance/block at the exact imaging plane as a functional alternative to pathological inspection. The main limitation of using EAM as the gold-standard for lesion comparison is that LAT-map conduction disruptions could ultimately only infer, not confirm, the presence of lesions. Also, EA maps are representative geometries of the cardiac chamber. The reproducibility and fidelity of the EA map to the actual anatomy and electrophysiology is largely dependent on various factors such as catheter stability, LAT-point acquisition density, and respiratory and cardiac motion. For example, figure 3C shows an RFA line that was incompletely anchored at the TA. LAT-conduction mapping at the annulus was sparse due to the difficulty of achieving stable catheter contact at the annulus. In this case, it was challenging to verify or deny an anchored lesion line from the LAT-map. The ARFI image (figure 3A) conclusively visualizes an unablated region at the TA that likely corresponds to the unanchored gap. Adding differential pacing to the methods may have improved the accuracy of these ambiguous EAM maps, but this was difficult to achieve in the small canine RA and was not performed in this study.

Assessing if the ARFI imaging plane was parallel and completely transecting a line of conduction block on the LAT-map was challenging; the difficulty was reflected in the moderate inter-reviewer agreement. LAT-maps could not provide information about lesion line thickness or irregular lesion morphology if the catheter drifted, making it difficult to predict the exact extent of RFA treatment based on the functional conduction map alone. Misalignment of the imaging plane through complete RFA lines and the corresponding alignment interpretation from the LAT-maps was likely a primary source of discrepancy between the ARFI imaging and EAM lesion assessments.

Conclusion

This study demonstrated that intracardiac ARFI imaging shows promise for evaluating RFA lesions during TCA. Reviewers of the ARFI images successfully identified RFA treatment and potential lesion line discontinuities. Further development of ARFI specific technology could increase the range of possible imaging depths, allow the imaging of oblique surfaces, and reduce the susceptibility of the images to motion artifacts. Successful clinical implementation of this technology could prompt operators to direct RF energy to incompletely ablated regions thereby enhancing lesion durability and reducing the need for repeat procedures.

Acknowledgments

Financial Support: Funding for this study was provided by NIH grant numbers R01-EB-012484, R21-EB-007741, and R37-HL-096023

We would like to thank Siemens Healthcare and Biosense Webster for their hardware system and support. We would also like to thank Joshua Hirsch, Stephen Hsu, Brittany Potter, Peter Hollender, Matt Brown, Veronica Rotemberg, and Mark Palmeri for their technical assistance.

Abbreviations

RFA	radiofrequency ablation
TCA	transcatheter cardiac ablation
AF	atrial fibrillation
EAM	electroanatomical mapping
ICE	intracardiac echo
ARFI	acoustic radiation force impulse
LAT	local activation time
CS	coronary sinus
EGs	electrograms
PIU	patient user interface
RA	right atrium
DOF	depth of field
FOV	field of view
MI	mechanical index
TA	tricuspid annulus
PPV	positive predictive value
NPV	negative predictive value
PV	pulmonary vein

References

1. Calkins H, Kuck KH, Cappato R, et al. HRS/EHRA/ECAS expert consensus statement on catheter and surgical ablation of atrial fibrillation: Recommendations for patient selection, procedural techniques, patient management and follow-up, definitions, endpoints, and research trial design. Heart Rhythm. 2012; 9:632–696.e621. [PubMed: 22386883]
2. Melby SJ, Lee AM, Zierer A, et al. Atrial fibrillation propagates through gaps in ablation lines: Implications for ablative treatment of atrial fibrillation. Heart Rhythm. 2008; 5:1296–1301. [PubMed: 18774106]
3. Kowalski M, Grimes MM, Perez FJ, et al. Histopathological Characterization of Chronic Radiofrequency Ablation Lesions for Pulmonary Vein Isolation. J Am Coll Cardiol. 2012; 59:930–938. [PubMed: 22381429]
4. Robinson MR, Hutchinson MD. Use of imaging techniques to guide catheter ablation procedures. Curr Cardiol Rep. 2010; 12:374–381. [PubMed: 20607626]
5. Nightingale K, Soo MS, Nightingale R, Trahey G. Acoustic radiation force impulse imaging: In vivo demonstration of clinical feasibility. Ultrasound Med Biol. 2002; 28:227–235. [PubMed: 11937286]
6. Pinton GF, Dahl JJ, Trahey GE. Rapid tracking of small displacements with ultrasound. IEEE Trans Ultrason Ferroelectr Freq Control. 2006; 53:1103–1117. [PubMed: 16846143]
7. Hsu SJ, Bouchard RR, Dumont DM, Ong CW, Wolf PD, Trahey GE. Novel acoustic radiation force impulse imaging methods for visualization of rapidly moving tissue. Ultrason Imaging. 2009; 31:183–200. [PubMed: 19771961]
8. Nightingale K, Bentley R, Trahey G. Observations of tissue response to acoustic radiation force: Opportunities for imaging. Ultrason Imaging. 2002; 24:129–138. [PubMed: 12503770]

9. Palmeri ML, Sharma AC, Bouchard RR, Nightingale RW, Nightingale KR. A finite-element method model of soft tissue response to impulsive acoustic radiation force. IEEE Trans Ultrason Ferroelectr Freq Control. 2005; 52:1699–1712. [PubMed: 16382621]
10. Nath S, Redick JA, Whayne JG, Haines DE. Ultrastructural observations in the myocardium beyond the region of acute coagulation necrosis following radiofrequency catheter ablation. J Cardiovasc Electrophysiol. 1994; 5:838–845. [PubMed: 7874329]
11. Bosman S, Pickering JW, van Marle J, van Gemert MJ. Ultrastructural alterations in heated canine myocardium. Lasers Surg Med. 1995; 17:39–48. [PubMed: 7564855]
12. Pernot M, Mace E, Dubois R, Couade M, Fink M, Tanter M. Mapping myocardial elasticity changes after rf-ablation using supersonic shear imaging. Computers in Cardiology. 2009; 2009:793–796.
13. Fahey BJ, Nightingale KR, McAleavey SA, Palmeri ML, Wolf PD, Trahey GE. Acoustic radiation force impulse imaging of myocardial radiofrequency ablation: Initial in vivo results. IEEE Trans Ultrason Ferroelectr Freq Control. 2005; 52:631–641. [PubMed: 16060512]
14. Hsu SJ, Fahey BJ, Dumont DM, Wolf PD, Trahey GE. Challenges and implementation of radiation-force imaging with an intracardiac ultrasound transducer. IEEE Trans Ultrason Ferroelectr Freq Control. 2007; 54:996–1009. [PubMed: 17523564]
15. Eyerly SA, Hsu SJ, Agashe SH, Trahey GE, Li Y, Wolf PD. An in vitro assessment of acoustic radiation force impulse imaging for visualizing cardiac radiofrequency ablation lesions. J Cardiovasc Electrophysiol. 2010; 21:557–563. [PubMed: 20021518]
16. National Research Council. Guide for the Care and Use of Laboratory Animals. 8. Washington, DC: The National Academies Press; 2011.
17. Nelson TR, Fowlkes JB, Abramowicz JS, Church CC. Ultrasound biosafety considerations for the practicing sonographer and sonologist. J Ultrasound Med. 2009; 28:139–150. [PubMed: 19168764]
18. Hsu SJ, Bouchard RR, Dumont DM, Wolf PD, Trahey GE. In vivo assessment of myocardial stiffness with acoustic radiation force impulse imaging. Ultrasound Med Biol. 2007; 33:1706–1719. [PubMed: 17698282]
19. Posner KL, Sampson PD, Caplan RA, Ward RJ, Cheney FW. Measuring interrater reliability among multiple raters: An example of methods for nominal data. Statist Med. 1990; 9:1103–1115.
20. Zar, JH. Biostatistical Analysis. Vol. Chapter 6.3. Englewood Cliffs, NJ: Prentice-Hall; 1974. p. 62-65.Heterogeneity Testing of 2×2 Tables
21. Nath S, Whayne JG, Kaul S, Goodman NC, Jayaweera AR, Haines DE. Effects of radiofrequency catheter ablation on regional myocardial blood flow: Possible mechanism for late electrophysiological outcome. Circ. 1994; 89:2667–2672.
22. Tai YT, Lee KL, Lau CP. Catheter induced mechanical stunning of accessory pathway conduction: Useful guide to successful transcatheter ablation of accessory pathways. Pacing and Clin Electrophysiol. 1994; 17:31–36.
23. Rostock T, O'Neill MD, Sanders P, et al. Characterization of conduction recovery across left atrial linear lesions in patients with paroxysmal and persistent atrial fibrillation. J Cardiovasc Electrophysiol. 2006; 17:1106–1111. [PubMed: 16911579]
24. Schwartzman D, Ren JF, Devine WA, Callans DJ. Cardiac swelling associated with linear radiofrequency ablation in the atrium. J Interv Card Electrophysio. 2001; 5:159–166.

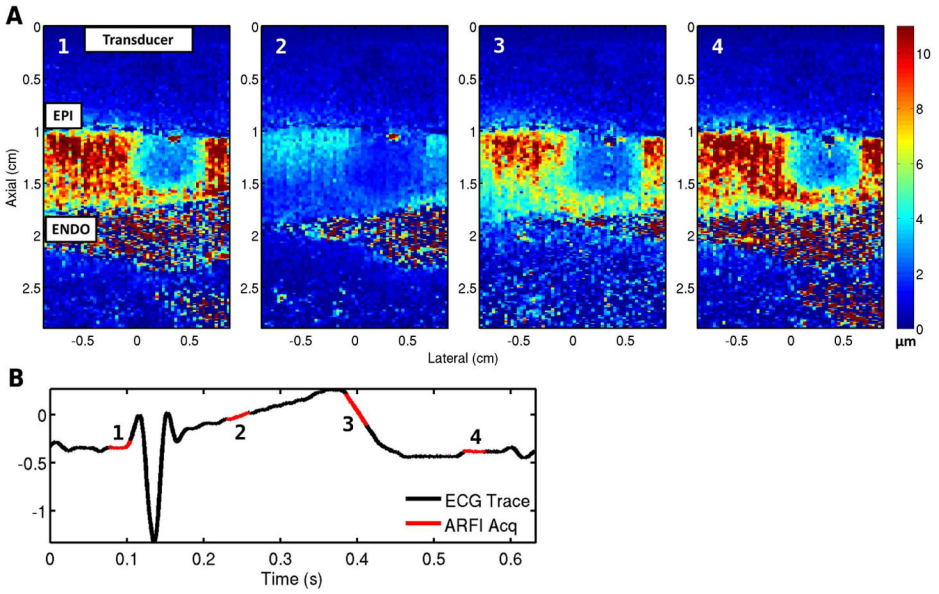

Fig 1.

ARFI images of a right ventricular epicardial RFA lesion through the cardiac cycle. Ablation catheter plane was vertically parallel to the page; the non-irrigated electrode tip ablated the epicardial surface (EPI = epicardium, ENDO = endocardium) for 7 sec at 20W. **A**) ARFI images acquired at different times during the cardiac cycle: (**1**) and (**4**) during diastole, (**2**) during systole, and (**3**) during end-systole. ARFI images were acquired with a linear transthoracic probe (VF10-5, Siemens© Medical) vacuum suctioned on the RV epicardium and imaging through a standoff. Color bar units are maximum displacement away from the transducer in microns; the transducer face is the top edge if the figure. Within the lesion the ARFI induced displacement is small (blue) throughout the cycle. The normal myocardium cycles between high displacement (red) during diastole and low displacement during systole. **B**) ARFI acquisition times corresponding to the ECG.

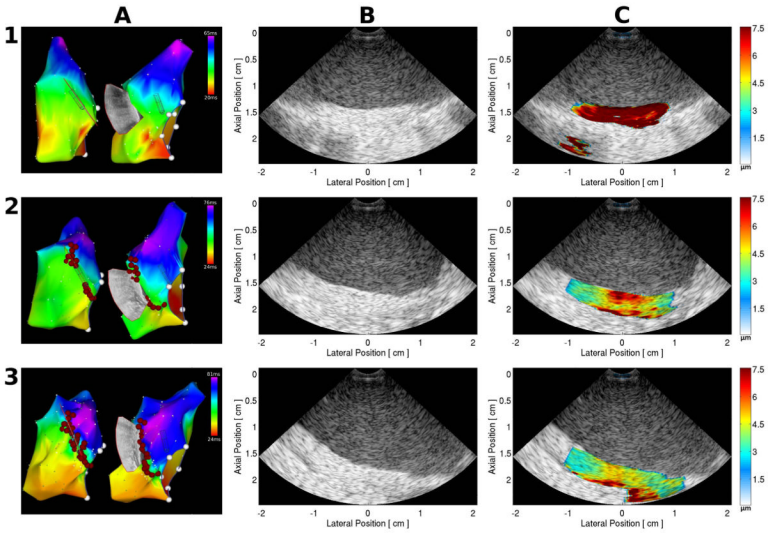

Fig 2.

An example of three ARFI image-LAT map pairs. **Row 1**) acquired before RFA, **row 2**) acquired after intentionally creating a 1 cm conductive gap, and **row 3**) acquired after closure of the 1 cm gap. **Column A**) LAT-maps showing the imaging fan position in the canine RA and the location of delivered RFA lesions (red spherical markers). **Column B**) conventional B-mode images acquired at the location indicated on the LAT-maps. There is no lesion visible in the B-mode images. **Column C**) Maximum ARFI-induced displacement images. The color bar units are microns of tissue displacement away from the transducer. RFA lesions sites are visible as regions of lower relative displacement (stiffer tissue), represented by the blue-green-yellow portion of the color bar.

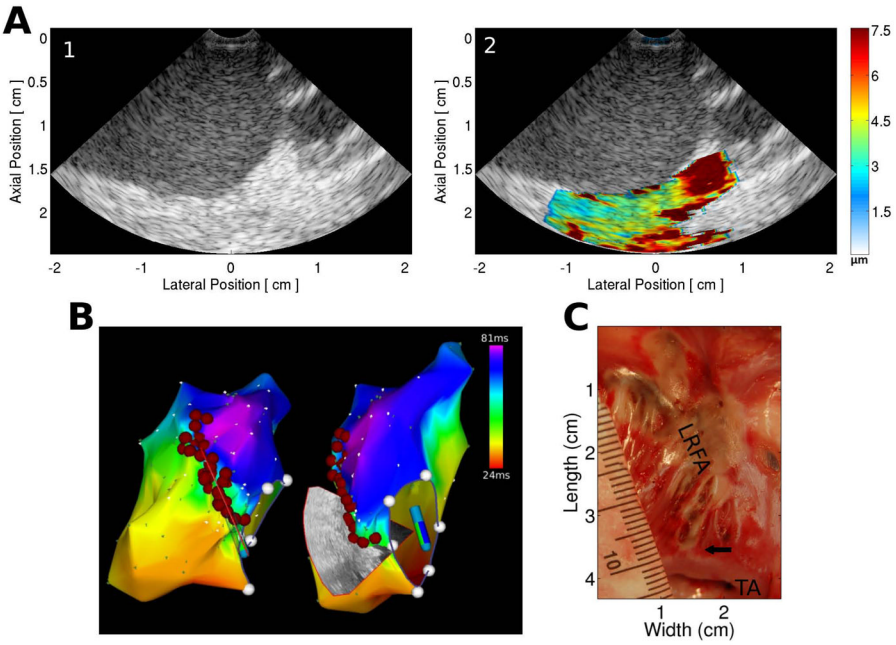

Fig 3.

A) Conventional (**1**) B-Mode and (**2**) ARFI image at the tricuspid annulus. The ARFI image shows an area of relatively high displacements at the annulus indicating a likely unablated region. ARFI image color bar units are microns displacement away from the transducer. **B**) LAT-map surrounding a line of RFA lesions in the RA, red spheres indicate RFA delivery sites **C**) Pathology photograph of the RA endocardial surface confirming continuous line of RFA lesions (LRFA). A small unablated gap is visible at the tricuspid annulus (TA), indicated by the black arrow.

Table I

ARFI image assessments for RFA treatment

		LAT-Map Assessment at Imaging Fan Location		
		No conduction disturbance	**Conduction disturbance inferring the presence of lesions**	**Total**
ARFI Image Lesion Assessment	No Lesion	54	6	60
	Lesion	5	134	139
	Total	59	140	199

Table II

ARFI image assessments for contiguous RFA

		LAT-Map Assessment at Imaging Fan Location		
		No block	**Block**	**Total**
ARFI Image Lesion Assessment	Non-contiguous lesion	67	27	94
	Contiguous lesion	22	24	46
	Total	89	51	140

Table III

Summary of statistical analysis for Tables I and II

	n	Heterogeneity χ^2	Heterogeneity P-value*	Sensitivity, %	Specificity, %	PPV, %	NPV, %
RFA Treatment (I)	199	4.59	0.7099	95.7	91.5	96.4	90.0
Contiguous RFA (II)	140	9.29	0.2325	47.1	75.3	52.2	71.2

*Heterogeneity analysis: DF = 7, do not reject H_O (eight samples are from a homogeneous population)